Demonstration of on sky contrast improvement using the Modified Gerchberg-Saxton algorithm at the Palomar Observatory

Rick S. Burruss*[a], Eugene Serabyn[a], Dimitri P. Mawet[a], Jennifer E. Roberts[a], Jeffrey P. Hickey[b], Kevin Rykoski[b], Siddarayappa Bikkannavar[a], Justin R. Crepp[c]
[a]Jet Propulsion Laboratory, California Institute of Technology, 4800 Oak Grove Drive, Pasadena, CA, USA 91109;
[b]Palomar Observatory, 35899 Canfield Road, Palomar Mountain, CA, USA 92060-0200;
[c]California Institute of Technology, 1200 East California Boulevard, Pasadena, CA USA 91125

ABSTRACT

We have successfully demonstrated significant improvements in the high contrast detection limit of the Well-Corrected Subaperture (WCS) using the Autonomous Phase Retrieval Calibration (APRC)[1] software package developed at the Jet Propulsion Laboratory (JPL) for the Palomar adaptive optics instrument (PALAO). APRC utilizes the Modified Gerchberg-Saxton (MGS) wavefront sensing algorithm, also developed at JPL[2]. The WCS delivers such excellent correction of the atmosphere that non-common path (NCP) wavefront errors not sensed by PALAO but present at the coronagraphic image plane begin to factor heavily as a limit to contrast. We have implemented the APRC program to reduce these NCP wavefront errors from 110 nm to 35 nm (rms) in the lab, and we have extended these exceptional results to targets on the sky for the first time, leading to a significant suppression of speckle noise. Consequently we now report a contrast level of very nearly 1×10^{-4} at separations of $2\lambda/D$ ***before*** the data is post processed. We describe here the major components of our instrument, the work done to improve the NCP wavefront errors, and the ensuing excellent on sky results, including the detection of the three exoplanets orbiting the star HR8799.

Keywords: phase retrieval, mgs, high contrast coronagraphy, wavefront sensing, adaptive optics, HR8799

1. INTRODUCTION

Directly imaging exoplanets orbiting very bright stars exposes significant technical challenges. The three exoplanets orbiting HR8799 were recently directly discovered using differential imaging on a large telescope[3]. Scattered star light emanating from uncorrected wavefront errors limit the contrast between star light and exoplanet light. These wavefront errors also push the detectable region where exoplanets can be seen further and further away from the host star. Depending on the chosen mask, most modern coronagraphs start to reach noteworthy contrast levels at angular separations from the center of the host star of about $10\lambda/D$ (where λ is the observing wavelength and D is the aperture diameter), giving large telescopes a distinct advantage to exoplanet detection. To detect faint stellar companions at smaller angular offsets, we need to significantly reduce the wavefront errors present in the imaging system, while efficiently blocking the star light and allowing the companion light to pass to the detector.

The residual wavefront errors that lead to the speckle noise which degrades contrast emerge from several sources. The adaptive optics instrument that delivers the wavefront to the science camera has a finite ability to correct for the turbulence in the atmosphere. Residual errors from this correction lead to speckles in the image which look like the planets we are trying to detect. In addition, errors at the science camera not sensed by the adaptive optics wavefront sensor camera contribute to the speckle noise. These NCP errors include differential image drift between the two cameras, differential focus between the cameras, and a quasi-static residual error due to small errors in the science arm induced primarily by flexure, brought on both by temperature gradients and changing gravity loads on the science arm as the telescope position is changed.

Our group commissioned an effort to reach the $1x10^{-5}$ contrast milestone at λ/D angular separations using the existing WCS, PALAO, and Palomar infrared science camera (PHARO). To effectively block the star light and allow for exoplanet detections very close to the host star we added the novel vector vortex coronagraphic (VVC) phase mask to the PHARO focal plane selector mechanism. To minimize image drift of the star from behind this mask during integrations we added new actuator mounts to the PALAO instrument. To reduce the NCP quasi-static wavefront errors we chose to incorporate the excellent APRC software package developed at JPL and implemented at Palomar Observatory in the lab in 2007. At that time APRC had only been demonstrated in the lab. We present here the work done to extend the APRC lab results to the sky. We also note the improvements gained by the new star selector mounts, and note that these mounts and the APRC updates are now available to all PALAO users. Finally we show that this work, coupled with the excellent performance of both the VVC mask and effective post processing techniques, allowed us to image the three exoplanet companions of HR8799.

2. THE WCS INSTRUMENT

The WCS instrument reimages a clear, 1.5 meter diameter, off-axis subaperture of the Palomar Hale telescope and delivers this reimaged wavefront to the PALAO instrument[4]. The resulting residual wavefront errors then passed on to the science detector are reduced from 200-250 nm rms when using the full telescope to 85-100 nm rms when using WCS. We use the PHARO near infrared camera for our work, and Palomar Observatory has graciously allowed us to add image plane and pupil plane masks to this camera. Note that any PALAO science camera can take advantage of the excellent correction provided by the WCS. We used the four-quadrant phase mask for our first high contrast experiments with the WCS and PHARO. While the resulting correction of the atmosphere was excellent, even providing suitable correction for visible images in the B-band, the speckle noise due to NCP wavefront errors limited the contrast ratio to $1x10^{-3}$. Image drift and target centering during these experiments was also a problem. Due to NCP flexure between PALAO and PHARO, we found that our targets drifted by 10 to 20 milliarcseconds (mas) per minute, requiring constant target position updates with mirror actuators whose smallest allowable offset was 22 mas steps. The uni-directional accuracy of these mounts was measured at 3 mas for commanded moves above 22 mas. Backlash of these mounts was a serious problem, so much so that if we changed direction of the target at all during an observation, the entire alignment process needed to be redone.

2.1. THE VECTOR VORTEX CORONAGRAPH

We recently installed a K-short band (2.15 μm) VVC phase mask in the PHARO focal plane to block the bright light of host stars[5]. We prefer phase masks because they are transparent and can transmit exoplanet light at small angular separations from the host star. Our VVC mask's theoretical half-power transmission occurs at 0.9λ/D from the center (about 260 mas in our case). A stringent tolerance on pointing and drift exists with these masks however, and needs to be accounted for. For example, given suitable wavefront correction at the focal plane where the mask resides, our VVC requires pointing to the center of the mask to be better than 0.02λ/D (about 5 mas in our case).

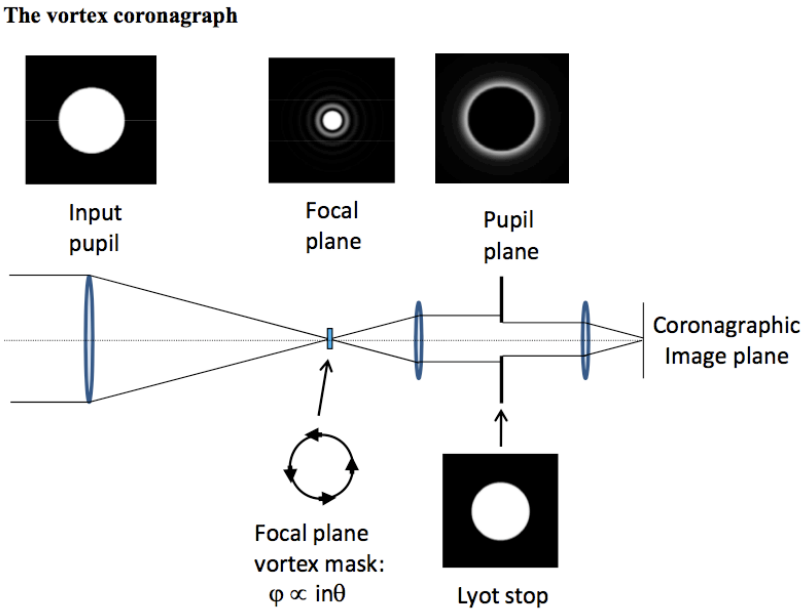

Figure 1. Conceptual layout of the Vector Vortex coronagraph: The light in the input pupil from PALAO is focused onto the PHARO focal-plane coronagraphic phase mask, for which the output phase, ϕ, is linearly proportional to the azimuthal angle, θ. In the vector vortex coronagraph the azimuthal phase ramp is induced by passage through a rotationally symmetric half-wave plate. After the vortex mask, the beam is recollimated, and in a subsequent PHARO pupil plane the starlight lies entirely outside the image of the original pupil (for a perfect wavefront), allowing the starlight to be rejected with an opaque, slightly undersized pupil stop (the Lyot stop).

2.2. PALAO IMAGE POINTING MOUNTS

To solve the pointing and drift problems, we purchased and installed new Aerotech[6] gimbal mounts to actuate the PALAO image pointing optics, replacing gimbal mounts that had been in service for nearly ten years. Aerotech's custom dual-encoded, motorized gimbal mounts were made for us to fit into the allowable space on the optical bench. During testing we immediately noticed a significant improvement in both image positioning and image drift caused by flexure. We also discovered a bug in our motor control software that nullified moves less than 22 mas. After fixing this bug, we tested small and large image motion commands and found that uni-directional image position accuracy is better than 2 mas. Bi-directional image position accuracy (backlash) is better than 3 mas. This excellent image positioning performance allows us to center targets on our mask quickly, and maintain the accurate positioning required by the VVC mask (5 mas) using small, accurate image motion commands.

Further, image drift due to flexure was vastly improved once these mounts were installed. Image drift using the new mounts is now measured at less than 1 to 2 mas per minute, depending on telescope position, significantly improving observing efficiency. Science targets are now quickly and efficiently positioned on the science camera. In our case, target acquisition has been reduced to a few minutes, as opposed to several tens of minutes. And once the target is centered on our VVC mask, keeping it there requires fewer target position updates since the NCP image drift has been so dramatically reduced. When observing on sky, we monitor the residual light scattered around the VVC mask in science images as they are displayed, which appears like a "doughnut" of light around the mask. At most telescope pointings where the image drift is less than 1 mas per minute, we issue a small, accurate correction to the new mounts once every 5 to 8 minutes to keep the target centered to within the 5 mas centering requirement of the VVC. We are now implementing a software algorithm to monitor the light leak from behind the VVC in PHARO science images, and then send image motion commands to PALAO to automatically keep targets centered on the VVC mask.

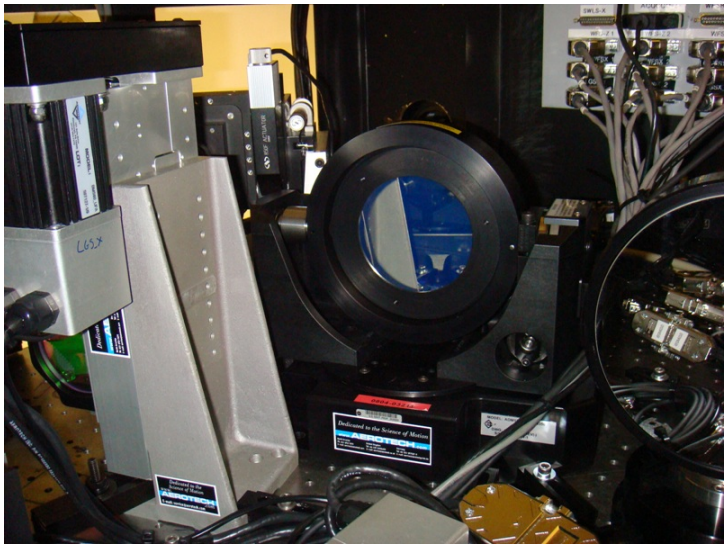

Figure 2. Custom Aerotech dual encoded gimbal mount: Star Selector Mount #1 in the PALAO instrument, which holds the science camera dichroic filter. The infrared light passes through this filter, while the visible light reflects to a mirror held in the other Aerotech gimbal mount. These two mounts are commanded in tandem to accurately move targets in both the PALAO and science instruments.

3. APRC UPDATES

APRC uses the PHARO science camera as the NCP wavefront measurement device. Two defocused images on either side of the camera's focal plane are taken of the internal white light source by moving the white light source stage and commanding PHARO to record images. These images are then sent to JPL for the MGS processing. The MGS result is an estimate that is converted into DM actuator voltages. These DM maps are then sent back to Palomar, applied to the DM, and the process is repeated until the NCP error is minimized. The entire process is done open loop with no high order correction applied. In 2007 APRC corrected the NCP residual error from 110 nm, which is the best that can be done by hand tuning, to below 40 nm rms. Due to complications converting these maps into the proper form that PALAO can use when the high order loops are closed, we were not able to use the MGS results on the sky.

In 2008 the PALAO optical bench was realigned to allow for larger science instruments. In addition to this realignment, a new all-reflective stimulus package containing a broadband white light source and alignment laser was installed to replace the original stimulus sources. Due to these changes to the optical path, a new set of APRC influence measurements was needed before we could consider moving APRC forward. Also, PALAO and PHARO had undergone several control software updates since APRC was first implemented. Communication and security protocols between Palomar and JPL had also changed. All of these issues were addressed in an attempt to streamline the APRC process into something that the Palomar night staff could use efficiently as a general PALAO observing tool.

3.1. APRC INFLUENCE MEASUREMENTS

The first thing we did was make sure APRC still worked. Due to several changes and upgrades to both PALAO and PHARO control software, a few APRC revisions were necessary to regain communication to the hardware in the lab. We fixed several communication issues between Palomar and JPL that had arisen due to security upgrades at Palomar. After this minimal effort to resurrect the APRC scripts, APRC was correctly measuring the NCP wavefront error in the lab.

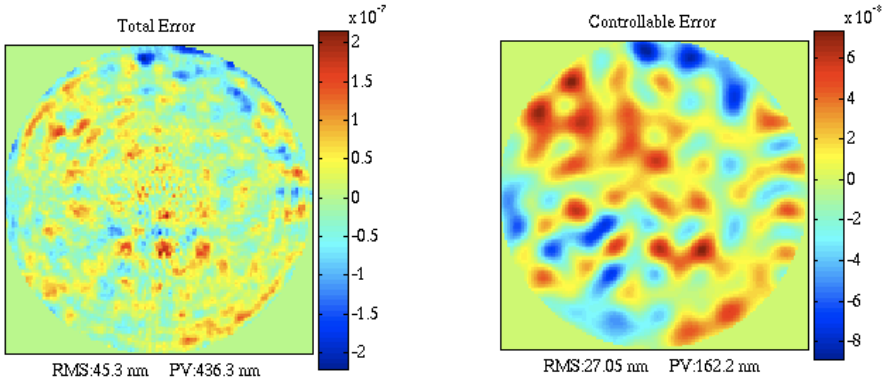

Figure 3. Preliminary APRC lab results: left. The total APRC residual error estimate after 4 iterations in February 2009 before any updates. The final residual NCP wavefront error is 45 nm rms **right.** The controllable APRC residual error estimate after the same 4 iterations. The controllable estimate is generated by passing the total error through a low-pass filter at 8 cycles per pupil. This is the residual error that the PALAO DM should be able to correct.

Next, using the APRC influence measurement tools developed in 2007, we re-measured the influence functions of the DM by poking DM actuators equal amounts in a grid pattern. We then took the standard set of defocused PHARO images of these grid patterns and used MGS to measure the wavefront effects of each poke. This combination of poke pattern data leads to a sensitivity matrix which is later used by APRC to convert the measured MGS wavefront error into DM voltages.

Under the guidance of the original APRC authors, we found that the MGS influence procedure can be affected by high dynamic range phase wrapping at the location of the DM pokes where low order aberrations in the wavefront are already unusually high. To reduce this effect, we ran several influence measurement trials at various DM poke heights (300, 275, 250, 225, 200 nm). We found that with DM pokes set to 250 nm, no phase wrapping occurred during our measurements. This 250 nm data set also produced the best results during the week that we tested in the lab, and so we have settled on this sensitivity matrix as the standard for APRC going forward.

In addition to measuring influence functions, we noticed that the APRC/MGS results are strongly coupled to air turbulence in the optical path. We have isolated some of this turbulence to air currents in the lab, and so have reduced some of the effects by covering the top of the exposed stimulus side of the PALAO bench. But some of the turbulence is still present in the optical path, and is not controllable. As a result, we experimented with longer PHARO exposure times, both for the standard APRC science exposures and for the exposures taken for these influence measurements. We found that in the lab (typically 70° F) the best results were obtained using exposure times of 30 seconds.

When an APRC iteration is completed, the result is displayed on the users screen which shows both the total measured NCP wavefront error and what we call the "controllable" wavefront error. The controllable wavefront error is simply the total error passed through a low-pass filter at 8 cycles per pupil, and is meant to convey the residual error that the DM should be able to correct (residual errors at frequencies higher than 8 cycles per pupil are not controllable by the DM). At first glance, a typical "best-case" APRC controllable error appears to show small bumps and valleys that look similar in size to a DM actuator, suggesting that actuators are not being controlled as well as desired, and perhaps there is something we can do about it. But when we overlay a map of the actuator positions that APRC determined during the influence measurements, we see that most of the controllable residual error in the inner 80% of the pupil exists between actuators. We also see that the centroiding algorithm that APRC uses to locate actuator pokes has trouble with poorly illuminated actuators at the outer pupil boundary, which may explain why the controllable error is higher in this region. We have not addressed this issue for this work.

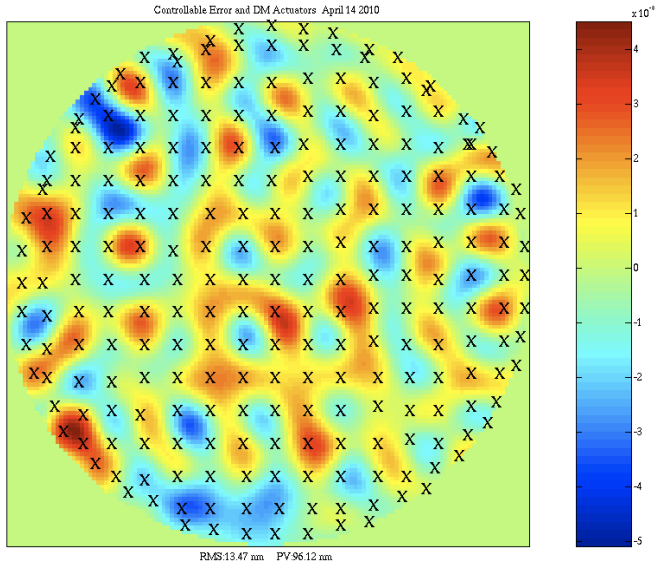

Figure 4. APRC Controllable Error: A best case APRC result from April 2010. The total APRC NCP wavefront error is passed through a low-pass filter at 8 cycles per pupil, showing what the PALAO DM should be able to correct. Overlaid on this residual error are the actuator positions that APRC determined during influence measurements. Note that most of the residual error in the central 80% of the pupil exists between DM actuators.

3.2. CLOSING THE LOOP WITH APRC

To extend the APRC results from DM actuator voltages to something we can use on sky, we derived a method to generate centroid offsets using the DM maps provided by APRC. With the solution applied to the DM, we close the high order loop with centroid offsets all set to zero. Centroid offsets are values subtracted from the measured centroids before commands are applied to the DM. The centroid offsets are in fact the values used to correct for NCP wavefront errors, and had been up to this point generated entirely by a manual hand tuning method, which for best case resulted in 110 nm residual wavefront error. With the centroid offsets set to zero, and the APRC solution applied to the DM, we lock the high order loop for 30 seconds. During this time the PALAO wavefront sensor camera measures the centroids generated by the APRC solution. We then extract these centroids, average them, and copy this result into a new centroid offset file. With this new centroid offset file loaded and the high order loop closed, the DM is now being commanded to the APRC solution, and we are now ready to go to the sky.

As local seeing conditions at Palomar change, the spot size of the target star in the wavefront sensor also changes. We know that as the spot size increases as seeing gets worse, PALAO performance may degrade when centroids are driven far from zero. We have learned that we can recover high order performance in most cases by using centroid offsets that have been divided by 2, and in some cases 4 or 6, such that the centroid slopes are retained but the amplitude of the deviations are reduced. Our APRC update generates these additional centroid offset files, which can be quickly loaded by the PALAO operator, and then verified by the observer before target observations begin.

3.3. TURBULENCE IN PALAO

We immediately noticed that the APRC/MGS solutions depend strongly on air turbulence and perhaps air temperatures in and around the PALAO bench when the APRC measurements are taken. We found that we could minimize the effect in the lab by tightly covering the top of the optical bench and turning the lab air conditioning blowers off. But we could not remove it completely, suggesting that some of the air currents in the PALAO bench cannot be controlled. We tried isolating hardware components to determine air current sources in the optical bench, but were not successful.

The APRC solution is a measurement of the difference of two defocused images. By default APRC commands the PHARO science camera to take as fast an exposure as possible (1.4 seconds) in order to reduce the total time it takes to finish an iteration. To better determine the proper exposure time necessary to reduce the air turbulence effects, we took long sets of open loop data with the PALAO wavefront sensor looking at the white light source. We extracted DM residual error wavefronts from this long data set. Using an approach very similar to an Allan variance, we subtracted averages of identical exposure times over the entire DM residual error data set (starting with one second). We then plotted the residual wavefront errors (rms) from these differences against the exposure time.

At the time of these tests the best controllable error we were seeing from APRC solutions was 15 nm ± 5 nm (rms). In the typical lab environment with tight covers on the optical bench, we found we could reach the 15 nm residual error level in 30 seconds. We adjusted APRC to command PHARO to take 30 second exposures at that time, and this has been the standard exposure time used for APRC. We have also collected similar data sets when on the telescope in ambient temperatures of 19° C (similar to the lab, but without tight covers on the PALAO stimulus) and 2° C. The plots indicate that exposure times closer to 60 seconds are required to reach the 15 nm residual error level when PALAO is on the telescope, likely because the tight cover over the stimulus must be removed when PALAO is installed. Further, when PALAO is exposed to very cold air as is typically the case in the winter months, these plots suggest that air turbulence is so strong that exposure times approaching 200 seconds are required to reduce the residual errors to the 15 nm level.

The entire APRC procedure now takes 5 minutes per iteration; 2.5 minutes to automatically move PALAO stage motors and to command PHARO to take exposures and move internal source mechanisms, and 2.5 minutes to automatically send the data to JPL, commence the MGS processing, and return the results to the PALAO control computer at Palomar. The entire procedure is now done via one command issued from a MATLAB session on the PALAO control computer. Three iterations are typically required to get to the noise floor when APRC is run in the lab or on the telescope if the dome air temperatures are above 10° C. The APRC/MGS noise floor in these cases is 13 nm ± 3 nm (rms). In the very cold winter months when ambient dome temperatures dip below 10° C, four to five iterations are required to reach the noise floor, and this floor is higher than when the temperatures are warmer. The APRC/MGS noise floor in the winter is 26nm ± 8 nm (rms), although we note that we don't have a lot of data in these conditions. We have tried 90 and 120 second exposure times in the winter months, but the 26 nm noise floor is not reduced in these cases, suggesting that perhaps the DM actuators do not perform as well in the cold temperatures. Further testing in these temperatures is required before we can say much more.

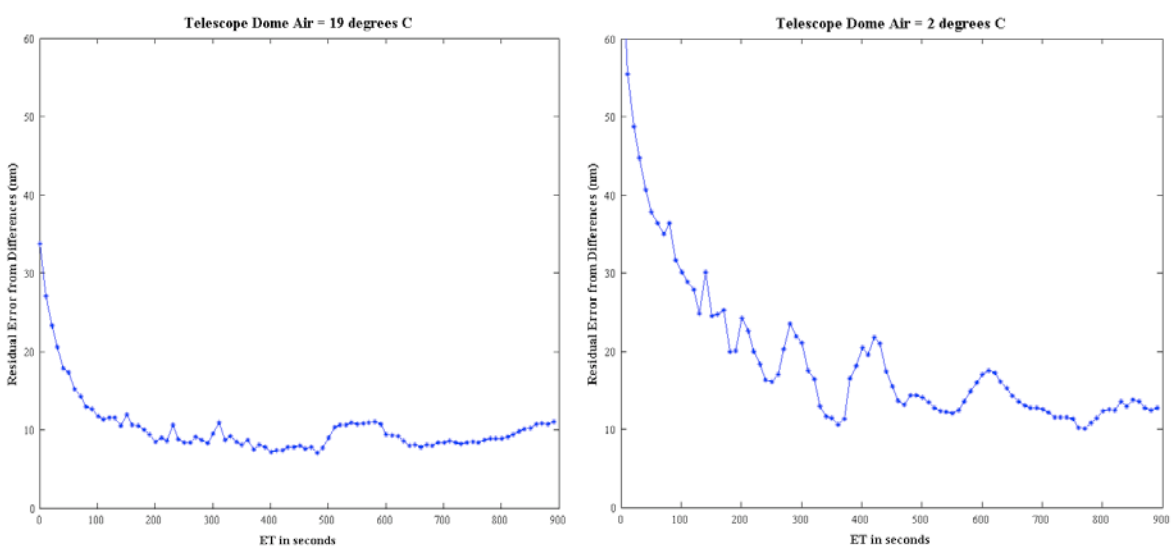

Figure 5. Air turbulence in the PALAO bench: left. Plot of the mean residual errors of differenced data sets against the exposure time used for that data set in the PALAO bench when installed on the telescope. The dome air temperature for this plot was 66° F. This plot suggests that 60 seconds is the ideal exposure time to reach the 15 nm residual error level. **right.** The same plot but with the dome air temperature at 35° F. This plot suggests that at least 250 seconds is the ideal exposure time to reach the 15 nm residual error level.

3.4. APRC FOCUS CONTROL

When APRC was first implemented in 2007, focus was allowed to pass into the APRC solution and so was propagated to the DM. In addition the measured focus in the solution was converted to linear stage units and printed to the screen so a user could move the white light internal stage to optimize the white light focus position before the next iteration. This was considered adequate as long as care was taken to make sure PHARO was focused manually (using a different procedure) before running APRC. To improve on this, we now use the APRC focus solution to automatically move both the white light stage and the PALAO wavefront sensor camera stage in equal but opposite amounts to effectively remove focus from the APRC solution, and keep focus off of the DM. These new motor stage positions are saved to the PALAO system settings so that they are always used if the system is stopped.

It is important to point out that MGS is an image tuning algorithm, which means we are using these methods to fine tune wavefront errors measured at the image plane of the detector. MGS does not measure wavefront errors at the PHARO focal plane where the coronagraph is located. High contrast performance requires superb wavefronts at the coronagraph, and so to benefit from MGS we need to ensure that the PHARO optical path between the focal plane and the image plane is as good as the PHARO design specifications say it is. To test this, we centered the internal white light source behind the VVC mask and we applied small amounts of low order Zernike's to the DM after the APRC solution is applied. We then looked for any changes to contrast. We did not find any measureable change to the contrast level at all, verifying the excellent quality in the optical path between the PHARO focal and image planes.

We have however measured a focus offset between the true PHARO focal plane and the position of the VVC phase mask, which was inserted into a clear substrate and mounted into the PHARO focal plane selector mechanism. We suspected that the mask was not located at the true focal plane, and so to test this, we positioned the PALAO internal white light source behind the VVC mask, and we looked at images taken in PHARO's pupil imaging mode. We noticed immediately a ring of scattered light illuminating the outer edge of the pupil images, which is what we would expect if the mask was not perfectly located in the PHARO focal plane. We then translated the PALAO wavefront sensor stage until the pupil image was nicely dark. We found that the offset between the VVC and the PHARO focal plane is corrected by a 400 μm translation of the PALAO wavefront sensor stage, and so we add this focus value to the stage when the APRC floor is reached.

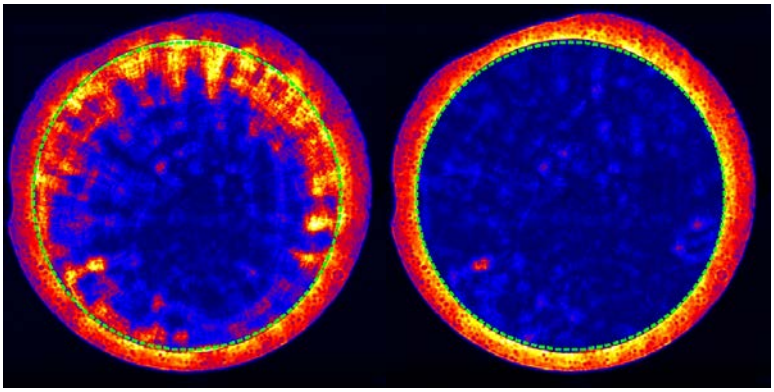

Figure 6. Before and after correcting the Vector Vortex focus offset: left. PHARO pupil image with the internal PALAO white light source centered behind the VVC mask. The wavefront entering PHARO is not correctly focused on the VVC mask, so some of the light is not blocked and is seen at the outer boundary of the pupil image. The green dashed line is the outer edge of the PALAO pupil. **right.** PHARO pupil image after translating the PALAO wavefront sensor stage 400 microns.

3.5. APRC ON THE TELESCOPE

In February 2010 we ran an APRC iteration at a non-zenith telescope position and noticed that this iteration reported a 40 nm rms increase in the wavefront error, suggesting that the total wavefront error changed simply by moving the telescope. We couldn't say at that time how much of the 40 nm increase was in the common path to both PALAO and PHARO, which would then be corrected by PALAO, or how much of this error was only in the NCP, which would not be corrected by PALAO.

In April 2010 we conducted a test to measure wavefront errors induced by non-zenith telescope pointings in such a way as to separate the common and non-common components. We started by running APRC on the white light at zenith and established the reference wavefront error at 22 nm rms. We copied the APRC solution into the reference PALAO flatmap (a map of actuator commands that leave the DM in the best possible open loop shape to create the best science image). We also generated centroid offsets on this map.

We then slewed the telescope to various telescope positions, starting in the east and slewing west, for each chosen declination. At each telescope pointing we ran one iteration of APRC on the white light, which measures the wavefront error through PALAO up to the science dichroic AND everything after the dichroic, including PHARO. We call this measurement the "total" error.

We then closed the high order loop on the white light (using the reference centroid offsets) and we let PALAO record a new flatmap. The difference of this flatmap to the reference flatmap taken at zenith measures the wavefront error through PALAO (as above) and everything reflected off of the science dichroic (the PALAO wavefront sensor arm). Assuming that the wavefront error through the wavefront sensor arm is small, we call this measurement the "common path" error.

The difference of the total error and the common path error is the non-common path error that is present at that telescope position. We found that for most telescope positions within 30° of zenith, the controllable residual NCP wavefront error is greater than 20 nm rms. And for telescope pointings beyond 30° of zenith, the residual NCP wavefront error is typically greater than 50 nm rms. We think this is due to gravity loads effecting optical mounts in the science arm. So to get the highest contrast possible at any non-zenith telescope pointing, APRC needs to be run at least once with the telescope pointed at the target location before observing. Note that APRC is always run on the internal white light source, it is not run on stars where the changing atmosphere adds phase errors to the raw data that bias the MGS result.

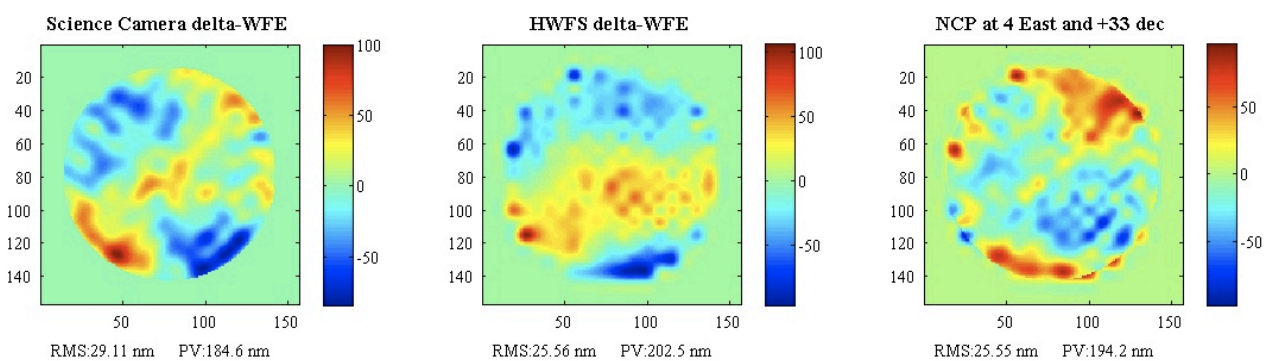

Figure 7. Wavefront errors with the telescope pointed to an hour angle of 4 hours East and a declination of +33°: left. The APRC solution measures a controllable difference of 29 nm rms between zenith and this telescope position. **middle.** The PALAO wavefront sensor solution measures a common path difference of 25 nm rms. **right.** The difference of these two measurements is the non common path error and is also 25 nm rms in this case. These images show that the errors induced by changing telescope positions are low order in nature, and so correctable by the DM. This strongly implies that APRC should be run at the beginning of each telescope position if high contrast performance is required.

3.6. APRC TODAY

APRC is now available to the entire PALAO observing community. The entire procedure is run by a single command executed on the PALAO control computer by the Palomar staff. It is a robust program that gives all PHARO users an on-sky wavefront quality improvement of a factor of 3 over that provided by the hand tuning method. APRC is also efficiently quick to provide wavefront improvements at various telescope positions for observers who require the absolute best corrections of the non-common path errors. The typical residual wavefront errors left over when APRC is done are remarkably low: 35 ± 4 nm rms total wavefront error, where 13 ± 3 nm rms remains in the controllable pass band of the deformable mirror.

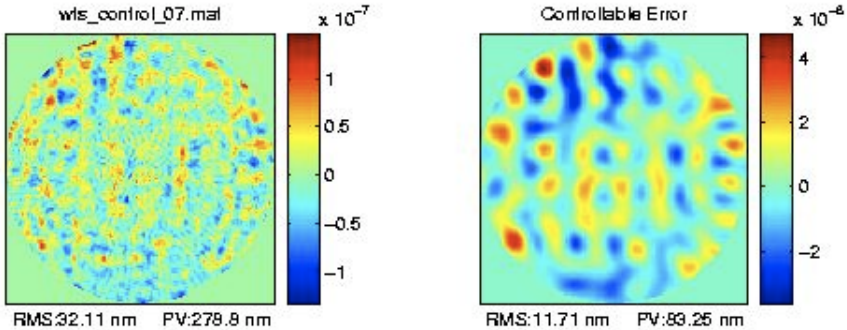

Figure 8. Typical APRC best case result: left. Usually after 3 iterations, APRC reaches a total error of 35 ± 4 nm rms **right.** The best case controllable error is 13 ± 3 nm rms.

4. ON SKY RESULTS

In the spring and summer of 2009 we took our first on-sky look at the benefits of coupling WCS, PALAO, PHARO and APRC together with the improved performance of the PALAO pointing mounts. In July 2009 we observed HR8799. For these observations we ran APRC during the evening just before opening the dome, but we did not run APRC at each target. We immediately noticed improved contrast in the raw VVC images, even though the seeing was a modest 1.6 arcseconds.

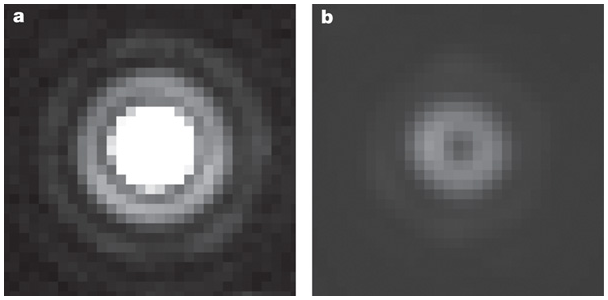

Figure 9. Pre and post-vortex HR8799 point spread function: a. The Ks-band raw stellar point spread function taken on July 11, 2009 with the WCS in 1.6" seeing. Strehl ratio is 0.91 ± 0.008 rms. **b.** The post vector vortex coronagraph point spread function on the same intensity scale. The peak to peak stellar rejection ratio is approximately 50, consistent with the observed Strehl ratio. Both images were taken with the same APRC solution applied to the high order correction. This APRC solution was acquired with the telescope at zenith earlier in the evening.

We also observe calibrator stars of similar magnitude and color to use as a reference to subtract the speckle noise from the target images. To do this effectively, the speckles need to remain constant between the target and the calibrator. We choose calibrators that are relatively close to the target star so that flexure does not introduce unwanted speckle noise in the images. As the telescope tracks across the sky, contrast is ultimately limited to the time it takes for the speckles to change significantly enough such that calibrator subtraction is no longer effective. Using data taken on HR8799 and other high contrast sources we have independently measured that a full magnitude of contrast is lost in about 8 minutes, strictly due to speckle decorrelation. For this reason we have implemented efficient telescope slew techniques to rapidly switch between targets and calibrators, keeping the total integration time to under 8 minutes for each position where possible.

4.1. POST PROCESSED RESULTS

Due to the excellent stability provided by the WCS and our efficient observing techniques, we were able to achieve nearly a full order of magnitude improvement in contrast using the "locally optimized combination of images" (LOCI) algorithm[7] to reference subtract calibrator stars from the target. In the case of HR8799, where both the target and two calibrator stars were observed for 800 seconds each, the fully reduced image shows all 3 known exoplanets clearly, including the innermost "d" planet whose separation from the host star is only 2λ/D (about 550 mas in our case).

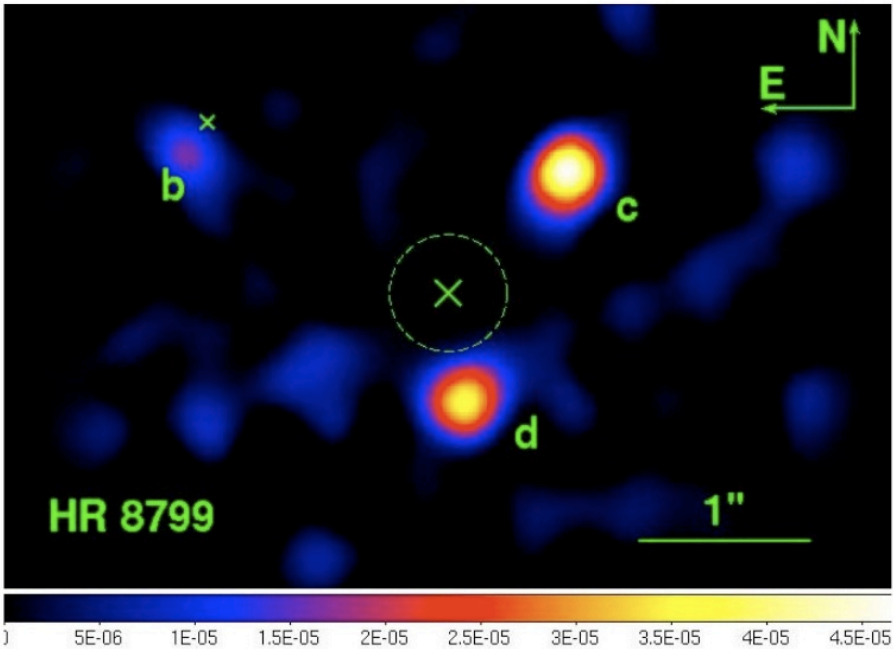

Figure 10. Final reduced image of HR8799: The fully reduced HR8799 exoplanet system after reference star subtraction using the LOCI algorithm. The innermost "d" exoplanet is located 2λ/D away from the center of the star. The central 1λ/D region is blanked out. The position of HR8799b from a 1998 Hubble observation is marked with an "x".

The contrast achieved in these images is remarkable. The APRC enhancements alone lead to an order of magnitude improvement in the residual speckle noise when combined with the VVC, contributing to the $1x10^{-4}$ contrast levels at 2.5 λ/D separations. After running the LOCI algorithm on the data sets, we are achieving contrast ratios of nearly $2x10^{-5}$ at the 4σ detection limit all the way in to λ/D separations, which is within a factor of two of the photon noise expected in the coronagraphic images.

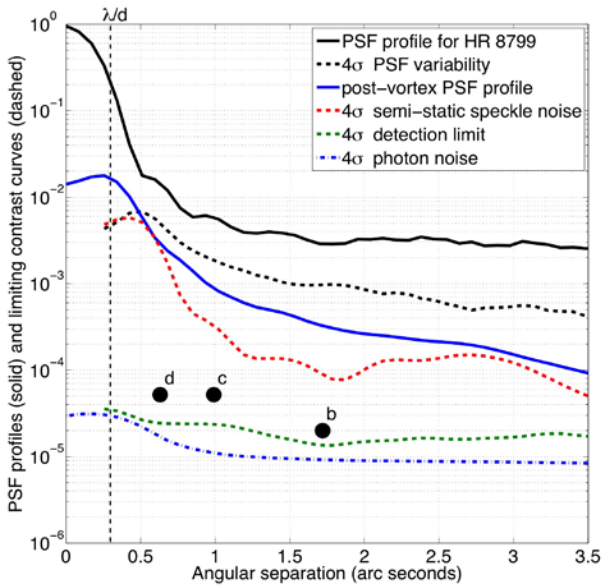

Figure 11. Azimuthally averaged point spread function profiles and limiting contrast curves: The top solid curve is the azimuthally averaged non-coronagraphic point spread function profile. The next solid curve (blue) is the azimuthally averaged post-coronagraphic residual point spread function profile. The top dashed curve is the 4σ azimuthal variations in the non-coronagraphic point spread function. The next dashed curve (red) shows the radial dependence of the post-VVC semi-static speckle 4σ noise level after using the APRC solution. The next dashed curve (green) shows the azimuthally averaged 4σ detection limit after reference start subtraction using LOCI. The next dashed curve (blue) shows the 4σ photon noise estimated from the residual stellar flux and the background.

5. FUTURE WORK

Our inner working angle is currently limited by residual high frequency tip tilt errors, which produces a halo around the center of the VVC mask. We will attempt to reduce these errors by manipulating the PALAO tip tilt servo gains during our next observing run. We also intend to implement an automated VVC centering algorithm that will monitor our raw coronagraphic PHARO images and adjust the PALAO image pointing to keep targets centered on our masks.

In the fall of 2010 the PALAO bench will be temporarily decommissioned for 6 months to upgrade to a 3000 actuator deformable mirror[8] (P3K). The new DM will work in tandem as a woofer - tweeter pair with the current 241 actuator DM. The APRC program will need to be updated to work with the new system. New influence measurements will need to be taken. And a new APRC interface to the entirely new P3K control software will need to be written.

The new P3K real-time software component operates on graphics cards to process the pixel data and control the 3000 actuators. Since we have a spare graphics card, and intend to install this card on the P3K operator's computer, we can conceivably run the MGS algorithms on site at Palomar on a graphics card. We ran MGS using data similar to our Palomar data on a graphics card at JPL, and note that the entire process takes 6 seconds, rather than 2 minutes. We intend to fully explore this option, which would mean APRC would be run entirely at Palomar in half the time it does now, and without the necessary internet connection to JPL.

6. ACKNOWLEDGEMENTS

This work was carried out at the Jet Propulsion Laboratory, California Institute of Technology, under contract with the National Aeronautics and Space Administration, and is based on observations obtained at the Hale Telescope, Palomar Observatory, as part of a continuing collaboration between the California Institute of Technology, NASA/JPL, and Cornell University. We thank the staff of the Palomar Observatory and the Palomar Adaptive Optics team for their continued support.

REFERENCES

[1] S. Bikkannavar, C. Ohara, M. Troy, "Autonomous phase retrieval control for calibration of the Palomar adaptive optics system", Proc SPIE, Vol. 7015, 70155K, (2008)
[2] J. Green, D. Redding, S. Shaklan, S. Basinger, “Extreme Wavefront Sensing Accuracy for the Eclipse Coronagraphic Space Telescope”, Proc. SPIE, Vol. 4860, 266-276, (2003)
[3] C. Marois, et. al., “Direct imaging of multiple planets orbiting the star HR8799”, Science 322, 1348-1352, (2008).
[4] E. Serabyn, et. al., “Extreme adaptive optics using an off-axis subaperture on a ground-based telescope”, Proc SPIE, Vol. 6272, 62722W, (2006).
[5] D. Mawet, et. al., “The Vector Vortex coronagraph: laboratory results and first light at Palomar Observatory”, Astrophysical Journal 709, 53-57, (2010).
[6] Aerotech, Inc., Pittsburgh, PA, United States, Phone: 1-412-963-7470, www.aerotech.com
[7] D. Lafreniere, et. al., "A new algorithm for point-spread function subtraction in high-contrast imaging: a demonstration with angular differential imaging", Astrophysical Journal 660, 770-780, (2007).
[8] A.H. Bouchez, et. al., "The PALM-3000 high-order adaptive optics system for the 5.1m Hale Telescope", Proc. SPIE, Vol. 7015, 70150Z, (2008).